Simulation of Semiconductor Processes and Devices 2016
Edited by E. Bär, J. Lorenz, and P. Pichler

Using One-Dimensional Radiosity to Model Neutral Flux in Convex High Aspect Ratio Structures

Paul Manstetten*, Lado Filipovic†, Andreas Hössinger‡, Josef Weinbub*, and Siegfried Selberherr†
*Christian Doppler Laboratory for High Performance TCAD at the
†Institute for Microelectronics, TU Wien, Gußhausstraße 27-29/E360, 1040 Wien, Austria
‡Silvaco Europe Ltd., Compass Point, St Ives, Cambridge, PE27 5JL, United Kingdom
Email: manstetten@iue.tuwien.ac.at

***Abstract*—We present a computationally inexpensive framework to compute the neutral flux in high aspect ratio structures during three-dimensional plasma etching simulations. It is based on a one-dimensional radiosity approach and is applicable to simulations of convex-shaped rotationally symmetrical holes and convex-shaped trenches of infinite length. The framework is intended to replace the full three-dimensional simulation step required to calculate the neutral flux during plasma etching simulations. Especially for high aspect ratio structures, the computational costs of the full three-dimensional simulation of the neutral flux at the desired spatial resolution conflicts with practical simulation time constraints. Our results are in agreement with those obtained using reference three-dimensional ray tracing simulations for various convex geometries. Within this framework, we present a comprehensive analysis of the influence of the geometrical properties of high aspect ratio structures as well as of the particle sticking probability on the particle flux.**

I. Introduction

In the context of NAND flash cell fabrication [1], the processing of high aspect ratio (HAR) holes is a key prerequisite. One of the processing steps used to fabricate HAR structures is ion-enhanced chemical etching (IECE) [2]. The simulation of such plasma etching processes requires the recalculation of the local neutral flux distribution on the surface at each simulation time step. This is necessary, because the surface may evolve at every simulation time step. For HAR structures, the local flux originating from re-emission is predominant and the local flux rates can easily vary by several orders of magnitude along the structure depth. At the spatial resolutions desired for practical simulation cases, this leads to very high computational costs for a conventional three-dimensional computation of the local neutral flux using Monte Carlo ray tracing [3] or radiosity based [4] methods. Therefore, we suggest to use a one-dimensional approximation for the calculation of the local neutral flux inside HAR structures.

We have recently introduced a one-dimensional radiosity approach for the calculation of the neutral flux in cylindrical holes [5]. A general formula for the view factor between the inner surfaces of two coaxial cone-like segments has been established, although until now it has only been applied to cylindrical holes. The radiosity equation has been formulated in a *receiving* perspective, which allows for fully adsorbing elements.

978-1-5090-0818-6/16/$31.00

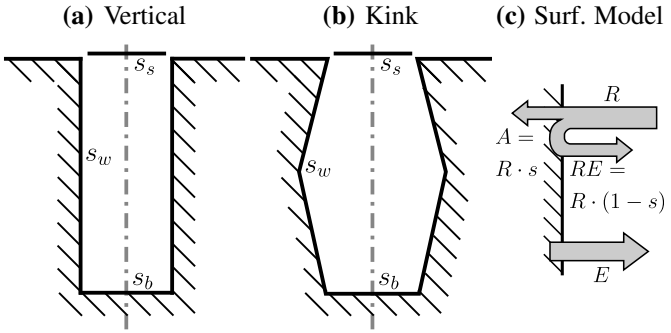

Fig. 1. Cross-sections of simulation domains with vertical walls (a) and with a kink at one half of the depth (b). s_s, s_w, and s_b designate the sticking probabilities for the source, the wall, and bottom region, respectively. (c) illustrates the surface model showing the relation between the received flux R, the adsorbed flux A, and the re-emitted flux RE; source areas emit flux E, which is independent of the received flux R.

In this work the one-dimensional radiosity approach is extended to handle convex-shaped rotationally symmetrical holes. Additionally, convex-shaped trenches of infinite length are introduced. We validate the resulting flux distributions along the wall and at the bottom of holes and trenches using a reference Monte Carlo ray tracing simulator [6]. Furthermore, we study the influence of geometric variations along the wall, as well as the variations of the particle sticking probability on the flux distributions.

II. Simulation Domain

For cylindrical holes, the simulation domain is a rotationally symmetric closed convex surface. For trenches, the simulation domain is a trench with a closed convex symmetric cross-section. The neutral flux source is modeled by closing the structures at the top. This leads to a disk-shaped source for holes and a strip-shaped source for trenches. Fig. 1a and Fig. 1b illustrate the cross-sections of domains with vertical walls and with a kink at one half of the depth, respectively.

The surface adsorption is modeled using a locally constant sticking probability s. The received flux R is split according to s into an adsorbed flux A and a re-emitted flux RE as depicted in Fig. 1c. Source areas additionally emit flux E independent of R.

For the remainder of this work, a sticking probability $s_s = 1$ is used for source areas, to prevent any influence of these areas on the flux distribution in the rest of the simulation domain. The bottom is modeled as a fully adsorbing area with a sticking probability $s_b = 1$. A constant sticking probability s_w is used for the walls of the structures. The choice of the wall and bottom sticking probabilities represents a reasonable approximation to the prevalent conditions for the neutral particles in an IECE environment.

III. Radiosity Formulation

The common assumptions for neutral particles, which also applies to our framework [5], is that all sources/surfaces are ideal diffuse and that the transport of the neutral particles is ballistic [7]; therefore, the use of a radiosity formulation is admissible. The prevalent radiosity formulation which is lined up to be solved for the radiosity (emitted + reflected energy) is not suitable for fully adsorbing areas; the radiosity vanishes for those areas and therefore the adsorbed energy cannot be recovered.

We use a formulation for the received flux. Assuming a constant flux and a constant sticking probability over each surface element, the received flux R for a surface element i is

$$R_i = \sum_j \left(E_j F_{ji}\right) + \sum_j \left(\left(1 - s_j\right) R_j F_{ji}\right) \tag{1}$$

and the relation to the adsorbed flux A is

$$A_i = R_i s_i, \tag{2}$$

where s is the sticking probability, E is the self-emitted energy, and F_{ji} is the view factor (proportion of the radiated energy, which leaves element j and is received by element i). Resolved for R and rewritten as matrix equation we obtain

$$\left(\mathbf{I} - \operatorname{diag}\left(1 - s\right) \mathbf{F}^T\right) \cdot R = \mathbf{F}^T \cdot E, \tag{3}$$

with the vector of emitted flux E, a vector of sticking probabilities s, and a matrix of view factors $\mathbf{F}$ (where F_{ij} corresponds to the view factor $i \to j$).

We approximate the solution of the resulting diagonally dominant linear system of equations (3) using the Jacobi method. Each iteration of the Jacobi method can be imagined as a concurrent diffuse re-emission of each element to all other elements. The adsorbed flux A is obtained by multiplying the entries in the solution for R with the corresponding sticking probability s of the element (2). The relation $\| A \| - \| E \| = 0$, which holds for closed surfaces, can be used to test the implementation and to define a stopping criterion for the Jacobi iterations.

IV. View Factors

To assemble the matrix of view factors $\mathbf{F}$ in (3) we must evaluate the view factors between all possible pairs of surface elements.

We discretize the surface of the structure into discrete elements along the line of symmetry. As an example, the shape of the resulting surface elements for a trench and hole are visualized in Fig. 2: two vertical ranges are indicated in Fig. 2b and the resulting surface elements a and b are shown for a trench and a hole in Fig. 2a and Fig. 2c, respectively. For the trench, each element is defined by two strips. For the hole, each element takes the form of a sliced cone.

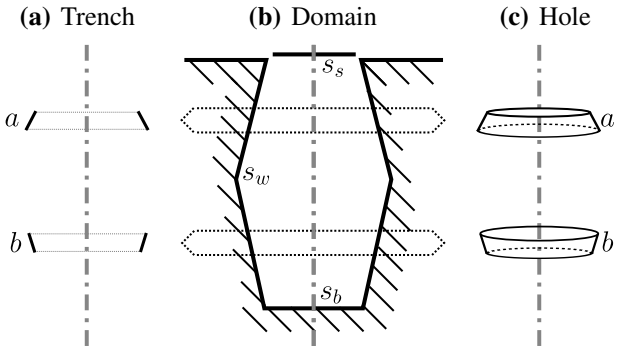

Fig. 2. Two surface elements which result when discretizing the domain (b) are displayed: (a) is the side view of two surface elements a and b, which results from a trench discretization and (c) is the isometric view of two surface elements a and b, which results form a hole discretization.

A. Trenches

The view factor between two segments of a symmetric convex trench with a constant cross section, as depicted in Fig. 2a, is derived using the crossed-strings method [8]. This method computes the view factor between two surfaces with a constant cross section and infinite length utilizing a two-dimensional re-formulation of the problem. For two mutually completely visible strips of infinite length the view factor is [8]

$$F_{1\to 2} = \frac{\left(d_1 + d_2\right) - \left(s_1 + s_2\right)}{2 \cdot a_1}, \tag{4}$$

where d_1 and d_2 denote the lengths of the diagonals when connecting the cross-section of the two strips to form a convex quadrilateral, s_1 and s_2 denote the lengths of the sides of that quadrilateral which connect the strips, and a_1 denotes the length of the side of the quadrilateral which represents the emitting strip.

Fig. 3a is a side view of the four strips from Fig. 2a. The view factors from the top right strip a_r towards the other three strips is visualized. The view factor between the two segments a and b is

$$F_{a\to b} = F_{a_r \to b_r} + F_{a_r \to b_l}, \tag{5}$$

where the subscripts denote the side of the strip according to Fig. 3a. a_l can be neglected, as the cross section is symmetric. The view factor of an element to itself is

$$F_{a\to a} = F_{a_r \to a_l}, \tag{6}$$

where again the reverse direction can be neglected due to symmetry. (4) is used to compute the view factors between individual strips in (5) and (6).

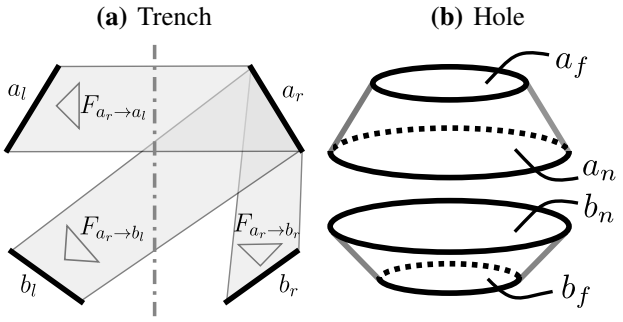

Fig. 3. Areas contributing in the view factor computation between two surface elements a and b. (a) Side view on the four infinite strips which correspond to the surface elements a and b from Fig. 2a; the view factors from strip a_r towards the other three strips are labeled. (b) Isometric view on two sliced cones which correspond to the surface elements a and b from Fig. 2c; the four limiting aperture disks are labeled.

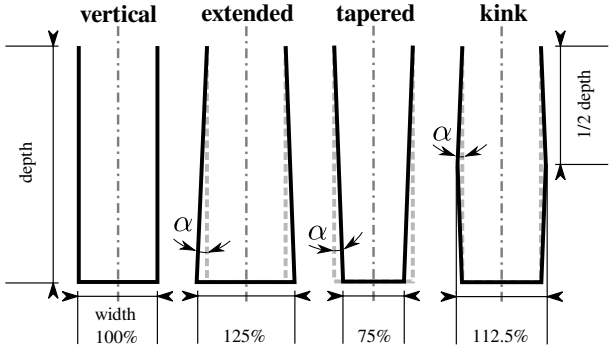

Fig. 4. Cross sections of the geometric variations of the wall for holes and trenches (shown for AR=3). Starting from a vertical wall, the bottom width is increased by 25% (extended) and reduced by 25% (tapered). Finally, the width at 1/2 of the total depth is increased by 12.5% to form a kink. The resulting angle α, which is identical for all three variations, is depicted.

B. Holes

In [5], we derive a general analytic formulation to compute the view factors between two segments of a rotationally symmetric convex hole as depicted in Fig. 2c. It is based on the view factor between two coaxial disks of unequal radii r_1 and r_2 at a distance z [9] and the reciprocity theorem of view factors. The final goal to compute the view factor between two elements a and b (compare Fig. 3b) is divided into multiple inexpensive analytic view factor computations between coaxial disks which mark the two limiting apertures of each element. This is possible as we only allow elements whose surfaces are mutually completely visible. For more details, the reader is referred to [5].

V. Results

The computed adsorbed flux in all of the following results is normalized to the flux which a surface of the same sticking probability would adsorb, if it is fully planar-exposed to the source. The aspect ratio (AR) is defined as $\frac{depth}{diameter}$ for holes and $\frac{depth}{width}$ for trenches.

In [5], we evaluated the quality of our one-dimensional radiosity model for cylinders of ARs 5 to 45 and sticking probabilities between 0.02 and 0.2. Good agreement was achieved when comparing to the results obtained with a reference Monte Carlo ray tracing simulator [6]. Extending this validation, several geometric variations (compare Fig. 4) including an extended, tapered, and kinked sidewall are applied to a trench and a hole with AR=25.

Fig. 5 shows the resulting flux distributions along the wall and at the bottom together with the reference results obtained from a Monte Carlo ray tracing simulation: good agreement is achieved. Due to the implicit representation of the surface in the ray tracing simulator sharp edges get smoothed out. This leads to differences near the wall-bottom interface, visible in Fig. 5b and Fig. 5d.

In Fig. 5a and Fig. 5c, the vertical dashed lines mark positions at 25% and 75% of the total depth of the structure, which are used as reference locations when comparing the wall flux in the following. For a sticking probability $s_w = 0.2$, Fig. 5a and Fig. 5b show small variations along the wall and at the bottom for both, holes and trenches; solely the presence of the kink clearly increases the flux on the bottom half of the wall compared to the vertical structure (about $+25\%$ at 75% of the total depth for both, trenches and holes).

When decreasing the sticking probability to $s_w = 0.01$, Fig. 5c indicates stronger deviations along the entire wall for all geometries. The variation of the wall-flux at 25% of the total depth is about $\pm 4\%$ for both, trenches and holes. At 75% of the total depth the variation is -7% to $+17\%$ for the holes and -7% to $+10\%$ for the trenches. Fig. 5d reveals a variation of about $\pm 25\%$ and $\pm 10\%$ for the flux at the center of the bottom in a hole and a trench, respectively.

Our simulation results show that low sticking probabilities increase the influence of geometric variations on the flux distributions along the wall and especially at the bottom of high aspect ratio structures.

VI. Summary and Outlook

We provide an approximation of the local neutral flux in three-dimensional plasma etching simulations of high aspect ratio structures using a one-dimensional radiosity approach. The framework presented in [5] is extended to handle convex-shaped trenches of infinite length. Comparing the results for various convex configurations using a rigorous three-dimensional Monte Carlo ray tracing simulation shows good agreement and applicability of our model for practical situations. We study the influence of geometric variations on the wall as well as the sticking probability on the flux distributions. The results indicate a strong influence for low sticking probabilities which are typical in IECE simulations of high aspect ratio structures.

Acknowledgment

The financial support by the *Austrian Federal Ministry of Science, Research and Economy* and the *National Foundation for Research, Technology and Development* is gratefully acknowledged.

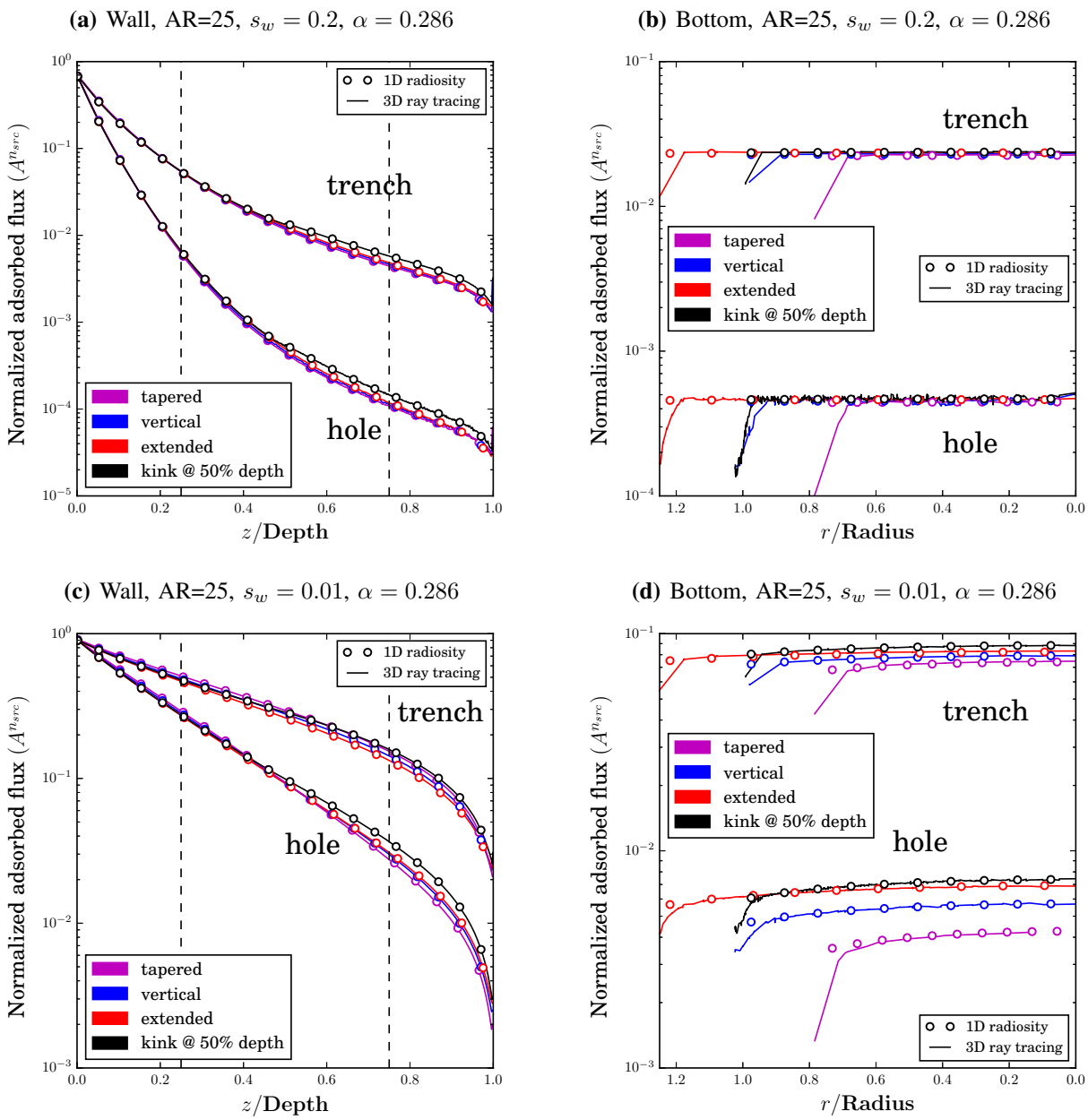

Fig. 5. Normalized flux distributions along the wall and at the bottom of a hole and a trench of AR=25 for sticking probabilities $s_w = 0.2$ (a) (b) and $s_w = 0.01$ (c) (d). The geometry of the structures is varied (according to Fig. 4); The results for structures with vertical sidewalls are plotted as a reference. Lines represent the results of the reference ray tracing simulator [6]. The deviations between ray tracing and radiosity towards the wall-bottom interface are due to the limited grid resolution of the ray tracing simulator. The flux distributions at the bottom span the interval [0.75,0] for the tapered structures and [1.25, 0] for the extended structures. In (a) and (c), the vertical dashed lines mark positions at 25% and 75% of the total depth.

References

[1] P. Dimitrakis, *Charge-Trapping Non-Volatile Memories: Volume 1 – Basic and Advanced Devices*. Springer, 2015.

[2] J. P. C. Francis F. Chen, *Lecture Notes on Principles of Plasma Processing*. Springer, 2003.

[3] O. Ertl and S. Selberherr, "Three-Dimensional Level Set Based Bosch Process Simulations Using Ray Tracing for Flux Calculation," *Microelectronic Engineering*, vol. 87, no. 1, pp. 20–29, 2010.

[4] T. Ikeda, H. Saito, F. Kawai, K. Hamada, T. Ohmine, H. Takada, and V. Deshpande, "Development of SF_6/O_2/Si Plasma Etching Topography Simulation Model Using New Flux Estimation Method," in *Proc. of SISPAD*, 2011, pp. 115–118.

[5] P. Manstetten, L. Filipovic, A. Hössinger, J. Weinbub, and S. Selberherr, "Using One-Dimensional Radiosity to Model Neutral Particle Flux in High Aspect Ratio Holes," pp. 120–123, 2016.

[6] O. Ertl, L. Filipovic, and J. Weinbub, "ViennaTS," https://github.com/viennats/viennats-dev, 2015.

[7] G. Kokkoris, A. G. Boudouvis, and E. Gogolides, "Integrated Framework for the Flux Calculation of Neutral Species Inside Trenches and Holes During Plasma Etching," *Journal of Vacuum Science & Technology A*, vol. 24, no. 6, pp. 2008–2020, 2006.

[8] M. F. Modest, *Radiative Heat Transfer*. Academic Press, 2013.

[9] J. R. Howell, M. P. Menguc, and R. Siegel, *Thermal Radiation Heat Transfer*. CRC press, 2010.